The STAGE method for simultaneous design of the stress and geometry of flexure mechanisms

Rommers, Jelle; van der Wijk, Volkert; Aragón, Alejandro M.; Herder, Just L.

DOI
10.1016/j.precisioneng.2024.05.021

Publication date
2024

Document Version
Final published version

Published in
Precision Engineering

Citation (APA)
Rommers, J., van der Wijk, V., Aragón, A. M., & Herder, J. L. (2024). The STAGE method for simultaneous design of the stress and geometry of flexure mechanisms. *Precision Engineering*, *89*, 103-112. https://doi.org/10.1016/j.precisioneng.2024.05.021

Precision Engineering 89 (2024) 103–112

Contents lists available at ScienceDirect

Precision Engineering

journal homepage: www.elsevier.com/locate/precision

The STAGE method for simultaneous design of the stress and geometry of flexure mechanisms☆

Jelle Rommers *, Volkert van der Wijk, Alejandro M. Aragón, Just L. Herder

Department of Precision and Microsystems Engineering, Faculty of Mechanical, Maritime and Materials Engineering, Delft University of Technology, Delft, The Netherlands

ARTICLE INFO

Keywords:
STAGE method
Flexure mechanism
Compliant mechanism
Stress design
Inverse FEM
Zero moment line

ABSTRACT

Current design methods for flexure (or *compliant*) mechanisms regard stress as a secondary, limiting factor. This is remarkable because stress is also known as a useful design parameter. In this paper we propose the Stress And Geometry (STAGE) method, to design the geometry of a flexure mechanism together with a desired stress field. From this design, the stress-free to-be-fabricated geometry is computed using the inverse finite element method. To demonstrate the potential of the method, the geometry of the well-known crossed-flexure pivot is taken as example. We first show how this mechanism can be redesigned for the same functional geometry with various internal stresses. This results for a specific choice of stress field in a design of a crossed-flexure pivot with 23% lower peak stresses during motion as compared to the known designs, for a ±45° rotation. We then present a second example, of a Folded Leaf Spring (FLS). With a parameter sweep the optimal stress field is calculated, showing a peak stress reduction of 28% during motion. This result was validated with an experiment, showing a normalized mean absolute error of 5.5% between experiment and theory. With a second experiment it was verified that the functional geometry of the FLS with internal stresses was equal to the one without internal stresses, with geometric deviations smaller than half the thickness of the flexures.

1. Introduction

Flexure mechanisms use elastic deformation of slender segments to achieve motion, which results in highly repeatable behavior due to the absence of friction and backlash. The design of these mechanisms is not trivial and multiple design methods exist, either based on degrees-of-freedom and constraints [1–3], rigid-body representations [4], the combination of simple building blocks to form more complex mechanisms [5–7], or structural optimization techniques [8].

The mentioned design methods focus mainly on the geometry of the mechanism and regard stress as a resulting, limiting factor. This is remarkable since stress is also known as a useful design parameter. Examples in engineering are the reduction of tensile forces in concrete by preloaded rods, avoidance of buckling by preloading bicycle spokes [9], and the preloading of bolts to mitigate their load cycle amplitude. Specific examples in the flexure mechanisms field are the introduction of clamping forces and elimination of backlash by a preloaded member [10], the introduction of multi-stable states using snap-through elements [11,12], and the reduction of stiffness using preloaded elements with negative stiffness [13,14].

A general method to design stresses in flexure mechanisms is not available, but various strategies to manipulate stresses for a specific geometric design are known. These strategies mainly aim to avoid stress concentrations. A first strategy is to opt for distributed instead of lumped compliance by using blade or wire flexures instead of notch hinges [8]. The stresses can be further smoothened by gradually increasing the thickness of the flexures at regions with stress concentrations [15,16], although this generally results in higher stresses in other regions due to the increased stiffness. Another strategy is to connect multiple flexures in series to reduce the required stroke of each element [17]. Although these strategies are effective, a major disadvantage they have is that the functional geometry originally intended by the designer is changed, leading to significantly sub-optimal designs.

In this paper we propose the Stress And Geometry (STAGE) method, to design the stresses and geometry of flexure mechanisms simultaneously. The functional geometry of the mechanism is designed together with a desired stress field for a certain pose of the mechanism, from which the stress-free, to-be-fabricated geometry is computed using the inverse finite element method.

☆ This paper was recommended by Associate editor Dr. Masonori Kunieda.

* Corresponding author.
E-mail address: j.rommers@tudelft.nl (J. Rommers).

https://doi.org/10.1016/j.precisioneng.2024.05.021
Received 3 November 2023; Received in revised form 2 May 2024; Accepted 30 May 2024
Available online 6 June 2024

Table 1
Properties of the CFP in Fig. 2.

Lx	100 mm
Ly	100 mm
w	30 mm
t_f	0.5 mm
t_r	10 mm
Young's modulus	114 GPa
Poisson's ratio	0.33

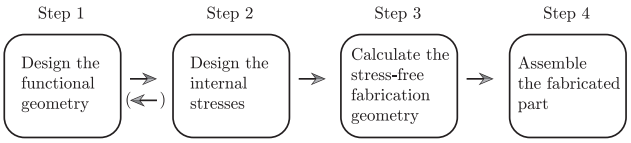

Fig. 1. Steps of the STAGE method to design the stresses and the functional geometry of a flexure mechanism simultaneously.

In Section 2, the STAGE method is presented and explained in detail, by applying it to the well-known crossed-flexure pivot (CFP) as an example. In Section 3 we demonstrate the potential of the method for designing a CFP with reduced peak stresses for large rotations, resulting in a new stress-free fabrication geometry. In Section 4, we present a second application example to reduce peak stresses, this time using a parameter sweep to find the most optimal stress field for a folded leaf spring. Two experimental tests have been conducted to validate the outcomes. In Section 5 we reflect on the results of the paper and in Section 6 we summarize the contributions of this work.

2. The STAGE method

The goal of the STAGE method is to simultaneously design the stresses and the functional geometry of a flexure mechanism. The method explicitly distinguishes between a *functional* geometry and a *fabrication* geometry. The functional geometry is what is generally regarded as the 'design' of a flexure mechanism. This geometry is in current literature usually unstressed. However, in this article the functional geometry usually exhibits stresses. If a functional geometry is allowed to relax, it attains the fabrication geometry, which exhibits no stresses and serves as drawing for production. Fig. 1 shows an overview of the method with four steps. In step 1 the functional geometry is designed. The focus in this step is on the kinematics of the mechanism, for which currently available design methods can be used. In step 2 the stresses in the mechanism are designed by determining the possible stress fields and selecting one. In step 3, the inverse finite element method is used to compute the stress-free fabrication geometry, required for production. At step 4, the fabricated shape is assembled, after which it attains the functional geometry while exhibiting the desired stresses. In between steps 1 and 2 there can be iterations in order to obtain the optimal functional geometry and internal stresses. The four steps will now be explained in detail. A video explaining the method can be found at https://doi.org/10.1016/j.precisioneng.2024.05.021.

2.1. Step 1: Design the functional geometry

The STAGE method starts with designing the functional geometry of the flexure mechanism. The focus in this step is on the kinematics of the mechanism, for which the currently available design methods can be used [1–8], for example to obtain a linear guide or rotational hinge with different functional geometries. Instead of designing something new in this paper, for explanation of the method we have chosen the well-known crossed-flexure pivot (CFP) in Fig. 2 as an example of a desired functional geometry. The CFP design dates back to at least 1948 and initially served to replace knife-edge bearings [15,18–20]. It consists of two thick plates connected by diagonal flexures. By bending of the

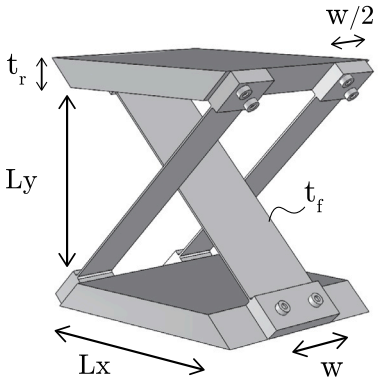

Fig. 2. The well-known crossed-flexure pivot (CFP) [15,18–20], which is chosen as example for explanation of the STAGE method.

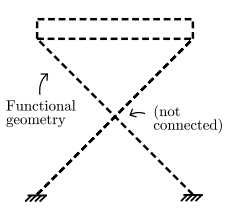

(a) Step 1: Design of the functional geometry.

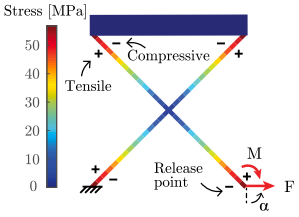

(b) Step 2: Design of the internal stresses by modeling a force and moment at a 'release point'.

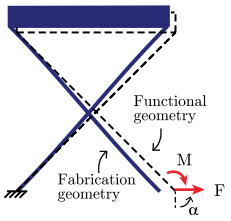

(c) Step 3: Calculation of the stress-free geometry for fabrication.

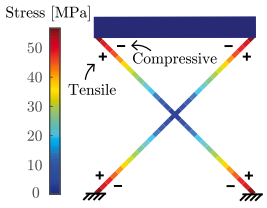

(d) Step 4: Assembly of the fabricated part to obtain the functional geometry with the desired stresses.

Fig. 3. The four steps of the STAGE method, explained with the crossed-flexure pivot. The geometry in the last step is the same as in the first step and exhibits the desired stresses.

flexures, the plates rotate with respect to each other. Table 1 shows the chosen properties of the CFP for this example. The lower plate is considered as the base.

Fig. 3 illustrates the four steps of the STAGE method, with the CFP design as the resulting functional geometry in step 1, modeled using a two-dimensional representation.

2.2. Step 2: Design the internal stresses

In step 2 of the STAGE method, the internal stresses of the flexure mechanism are designed for a certain pose of the mechanism. In this case the central pose is selected. To introduce the stresses, a 'release point' is defined, where the mechanism is virtually cut open and where a force and moment are modeled, as shown in Fig. 3(b). The force and moment define the stresses in the mechanism and will also be the input for step 3 in which the fabrication geometry is calculated. In this section we present a graphical approach which helps to relate the stress fields and the modeled force and moment. We start with a single blade

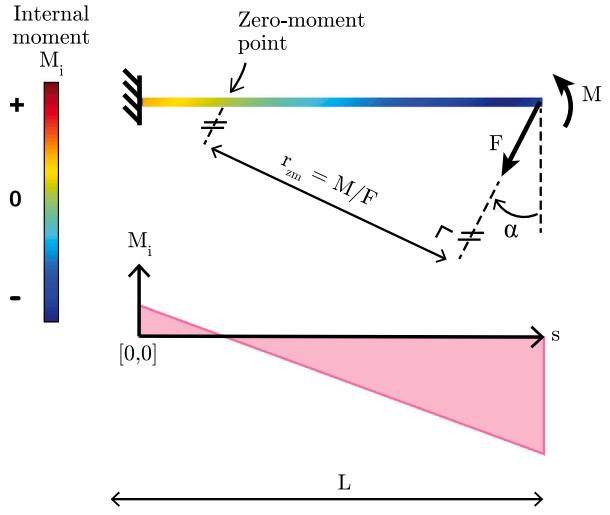

Fig. 4. The internal moment distribution (bottom) in the cantilever beam (top) can be modified by the applied force and moment. For slender beams, this distribution is proportional to the stress field.

flexure, then generalize the theory to a more complex flexure system and finally apply the theory to the CFP.

In a two-dimensional representation, a blade flexure is essentially a slender beam in which stresses are induced by moments and transverse and axial forces. In general, the stresses in such a slender beam are dominated by its internal moments [21], and can be computed as [21]:

$$\sigma = M_i \frac{t_f}{2I}, \tag{1}$$

where σ is the maximum stress in the cross section, M_i is the internal moment in point i of the beam, t_f is the thickness of the beam, and I is the area moment of inertia belonging to the bending direction. Eq. (1) shows that the stress and internal moment have a proportional relation which is solely dependent on the cross section of the beam. This means that we can use internal moments to visualize the stresses in flexure mechanisms if these are composed of slender flexures. An exception is the case where axial forces are significantly higher than the transverse forces, such that the pressure due to the axial force is in the same range as the bending stresses from Eq. (1).

In Fig. 4, a slender cantilever is illustrated, representing a blade flexure subjected to a force and moment. The graph shows its internal moment, derived using static equilibrium as [21]:

$$M_i(s) = cos(\alpha)F(L-s) - M, \tag{2}$$

where s is the coordinate along the length axis, L is the length of the beam and α is the angle of the force, as indicated in Fig. 4. The moment graph is a linear function. Also, it is independent of the cross section and stiffness of the beam because the system is statically determinate: the internal moments can be derived using solely static equilibrium equations.

Fig. 5 shows how this theory applies to a slender beam with arbitrary curvature. The beam is considered fixed at the bottom left corner with a force F and a moment M acting in the right extremity of the beam. Here the internal moments are represented by a linear field, with colors depicting the values. For any point i along the beam (and also in any point within the rest of the field) the internal moment can be calculated as:

$$M_i(r) = Fr - M, \tag{3}$$

where r is the moment arm between the point i and the line of action of the modeled force F. The line of points where $M_i(r)$ is zero is named

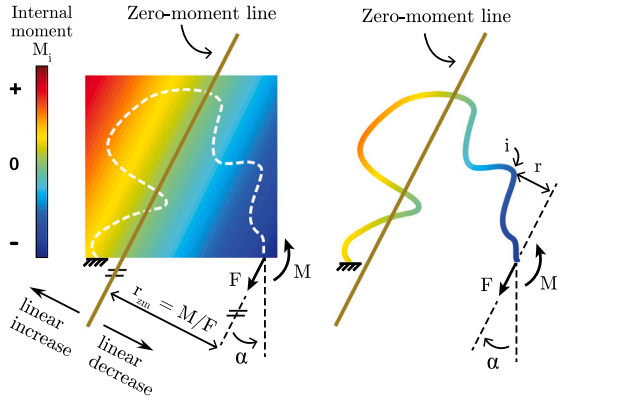

Fig. 5. The internal moment field in an arbitrarily curved beam can be modified by means of a force F and a moment M in a point of the beam. The moment field is linear and can be visualized using the zero-moment line. (For interpretation of the references to color in this figure legend, the reader is referred to the web version of this article.)

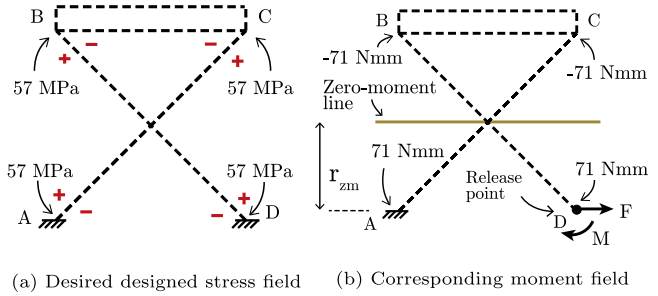

Fig. 6. (a) The desired stress field defined at four points, where the plus and minus signs indicate tensile and compressive stresses at each side of the flexures; (b) Internal moments calculated from the stress field, with corresponding zero-moment line from which the modeled force and moment are derived.

the "zero-moment line" as illustrated in Fig. 5. This is a unique feature in the visualization of the moment field.

Three design rules can be defined, relating the moment field to the modeled force and moment:

Rule 1. *The zero-moment line is always parallel to the direction of the modeled force.*

Two points in the field will experience the same internal moment if they have the same moment arm r with respect to the direction of the modeled force, as can be derived from Eq. (3). This also relates the points with zero moment.

Rule 2. *The distance between the zero-moment line and the line of action of the modeled force is* $r_{zm} = M/F$.

For points with moment arm $r = r_{zm}$ in Eq. (3), the moment applied at the end of the beam is in equilibrium with the moment due to the force at the end of the beam. Therefore the internal moment (and the bending stress) is zero at these points.

Rule 3. *The gradient of the moment field in the direction perpendicular to the zero-moment line is equal to the magnitude of the modeled force.*

Eq. (3) shows that the moment field is linear with a gradient of $\partial M_i/\partial r = F$.

We will now demonstrate the theory by designing the stresses in the CFP. First, a desired stress field is converted to a moment field, which is then used to calculate the required force and moment in a chosen release point. Suppose that we want the CFP to exhibit the

stress field shown in Fig. 6(a) (in Section 3 we will show that this particular stress field results in decreased peak stress during motion, compared to the traditional CFP design). A stress of ±57 MPa is defined in the four extremities of the flexures and between these points the field is assumed to be linear. The plus and minus signs indicate tensile and compressive stresses at the sides of the flexures, respectively. We convert these desired stresses into internal moments using Eq. (1) and the parameter values in Table 1, which yields the moment field shown in Fig. 6(b). A release point is chosen at the bottom right corner since this is a practical place to intersect the mechanism and assemble it after production of the fabrication geometry. Theoretically, however, any point in the mechanism could be chosen as a release point. The zero-moment line shows to be horizontal, laying in the middle of the four extremities as indicated. The distance between the zero-moment line and the release point therefore is $r_{zm} = L_y/2 = 50$ mm. Then, following design rule 1, the modeled force in the release point should be parallel to the zero-moment line, which means that it should be horizontal in this case. The magnitude of the modeled force is equal to the gradient of the moment field according to rule 3, which yields $F = 71$ N mm/50 mm = 1.42 N. The modeled moment is calculated using the relation $r_{zm} = M/F$ from design rule 2, resulting in $M = -71$ N mm, which is correct because it is the opposite of the internal moment in that point.

2.3. Step 3: Calculate the stress-free fabrication geometry

In step 3 of the STAGE method, the stress-free fabrication geometry is computed. This is an inverse problem since from the stressed functional geometry with the modeled forces and moments acting on it, the stress-free geometry has to be obtained. If the deflections are sufficiently small, the stress-free geometry can be calculated using linear beam theory. However, if the deflections are large and no analytical solution is available, nonlinear inverse FEM can be used. Originally proposed in [22], inverse FEM was introduced to the flexure mechanisms community by [23]. The authors use finite beam elements, which are specifically suited for flexure mechanisms. In this section we start by explaining regular nonlinear FEM, and then show the difference with inverse FEM. Because the solution method is somewhat counter-intuitive, an illustrative example for a rigid-body mechanism is provided in Appendix A.

In FEM, the investigated geometry is first discretized and represented with (beam) finite elements connected by nodes. The goal is to solve a residual equation containing a force imbalance, which is described as

$$\mathbf{R}(\mathbf{U}) = \mathbf{F}_{int}(\mathbf{U}) - \mathbf{F}_{ext} = \mathbf{0}, \tag{4}$$

where $\mathbf{U}$ is the displacement vector containing nodal translations and rotations. For large deflections, $\mathbf{F}_{int}(\mathbf{U})$, and therefore $\mathbf{R}(\mathbf{U})$, is in general nonlinear. The solution to the residual equation can be found iteratively using Newton–Raphson with the gradient

$$\mathbf{K} = \frac{\partial \mathbf{R}(\mathbf{U})}{\partial \mathbf{U}}. \tag{5}$$

The residual equation in Eq. (4) is written in terms of the displacement vector $\mathbf{U}$. To explain the difference between forward and inverse FEM, it is useful to write the residual equation in terms of the unstressed and stressed geometries instead. This can be done using the fact that the displacements are the difference between the stressed and the unstressed geometries. This means that:

$$\mathbf{U} = \mathbf{X}_s - \mathbf{X}_0, \tag{6}$$

where $\mathbf{X}_0$ and $\mathbf{X}_s$ are vectors containing the nodal coordinates and rotations of the stress-free and stressed geometry, respectively. We can now rewrite the residual equation as:

$$\mathbf{R}(\mathbf{X}_0, \mathbf{X}_s) = \mathbf{F}_{int}(\mathbf{X}_0, \mathbf{X}_s) - \mathbf{F}_{ext} = \mathbf{0}. \tag{7}$$

For regular, forward FEM, $\mathbf{X}_0$ is known and $\mathbf{X}_s$ can be found using the gradient of the residual equation

$$\mathbf{K}_{fwd} = \frac{\partial \mathbf{R}(\mathbf{X}_0, \mathbf{X}_s)}{\partial \mathbf{X}_s}. \tag{8}$$

For inverse FEM, on the contrary, $\mathbf{X}_s$ is known and $\mathbf{X}_0$ has to be found. We again use the gradient of the residual with respect to its unknowns, which is in this case

$$\mathbf{K}_{inv} = \frac{\partial \mathbf{R}(\mathbf{X}_0, \mathbf{X}_s)}{\partial \mathbf{X}_0}. \tag{9}$$

The residual equations of the forward and inverse analysis are the same, but different variables in the equation are unknown. Because of this, a different gradient needs to be computed to find the solution, while the rest of the calculations are similar for both analyses.

Instead of inverse FEM analysis, also regular nonlinear optimization methods for compliant mechanisms could be used to compute the stress-free geometry. However, in comparison the inverse FEM has a significantly lower computational cost since the nonlinear residual equations have to be solved only once [23].

2.3.1. Matlab model

Using the method described in Section 2.3, a FEM code was written in Matlab for the computations in this article. We will refer to this as the "Matlab model". The computations are checked using the commercially available software package Ansys and by experiments, in Sections 3 and 4.

2.4. Step 4: Assemble the fabricated part

In step 4 of the STAGE method the stress-free fabricated mechanism is assembled. As shown in Fig. 3(d), it attains the functional geometry of step 1, and exhibits the desired stresses of step 2. The reactions on the lower right attachment point are equal to the force and moment modeled in the release point in step 2. We have now obtained a flexure mechanism with both a designed geometry and designed internal stresses.

2.5. Discussion on the STAGE method

Instead of using the STAGE method, direct prestress could be used to introduce stresses in a flexure mechanism. However, this will change its designed, functional geometry. For example, a flexure which is designed and fabricated as a straight member will become curved after pre-stress, which severely decreases its off-axis stiffness (stiffness in the supporting directions). Using the STAGE method, the functional geometry is unchanged after assembly.

The moment field in step 2 is independent of the functional geometry if the mechanism is statically determinate, because in that case the moments are fully determined by static equilibrium equations. For example, the stiff bar in the CFP does not change the moment field. The same holds if its flexures would have different cross sections. Note however that in that case, a different proportionality between stress and moments has to be taken into account, according to Eq. (1): thicker flexures subjected to the same moment will experience a lower stress. The independency of the moment field also allows to reconsider the functional geometry in step 2. If a flexure is drawn in a certain moment field, it will attain the moment values of that field. This way, regions which are sensitive to fatigue failure could be designed such that they are close to the zero-moment line, and therefore experience lower bending moments.

The method to design the stresses in step 2 can be used directly if the mechanism is statically determinate, such as for the CFP. For statically indeterminate mechanisms, an approach can be to isolate a part of the mechanism such that a statically determined sub-mechanism is obtained. Alternatively, theory on statically indeterminate beam structures could provide a solution [21]. These approaches rely on stiffness and compatibility equations. If these approaches also do not suffice, a parameter sweep could be used. We will demonstrate this in Section 4.

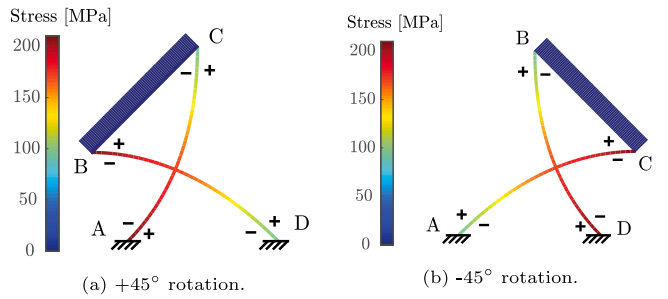

Fig. 7. FEM simulations show the peak stresses of 210 MPa in the traditional CFP for large rotations.

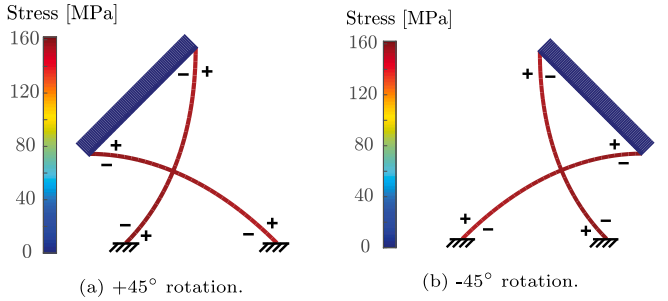

Fig. 8. FEM simulations of the redesigned CFP showing peak stresses of 161 MPa, which is a reduction of 23% compared to the traditional design. The fabrication geometry is shown in Fig. 3(c).

3. Application example: CFP with reduced peak stress

In this section we use the STAGE method to decrease peak stresses in the traditional CFP design during motion. The goal is to demonstrate one of the possible applications of the method. We first analyze the peak stresses of the traditional CFP at large rotations. From this, we determine a desired stress field which the CFP should exhibit in its central position. This stress field is introduced using the STAGE method. We then compare the stress peaks during motion of the traditional and the redesigned CFP. The outcomes are validated using the commercially available FEM software Ansys.

For large rotations, the flexures of the traditional CFP experience stress peaks close to their extremities, as shown in the FEM simulations in Fig. 7. The plus and minus signs indicate the tensile and compressive stresses at the sides of the flexures, respectively. The stress in point A ranges from −209.7 MPa to +96.05 MPa throughout the rotation. The peak stress can be reduced by introducing half of the difference, +56.83 MPa, at point A when the CFP is in its central position. This desired stress is shown in Fig. 6(a). The desired stresses in points B, C and D have been determined using the same reasoning. Following Sections 2.2, 2.3 and Fig. 3, the required stress-free fabrication geometry is obtained. After assembly, the redesigned CFP exhibits the stresses shown in Fig. 3(d) in its central position. At ±45° rotation, it exhibits the stresses shown in Fig. 8. As compared to the traditional CFP, the stress field is significantly smoother and the peak stresses are 161 MPa, which is a reduction of 23%.

The FEM results in this section are obtained using the FEM code written in Matlab in order to do the inverse computations, as described in Section 2.3. The results were verified using Ansys as follows. First the fabrication geometry (shown in Fig. 3(c)) was imported in Ansys, virtually assembled and rotated 45° back and forth. The peak stresses, occurring anywhere in the mechanism and anywhere in the motion range, were recorded. Beam elements of type “Beam 188” have been used, and the nonlinear analysis option was enabled. The stresses of the traditional CFP were also computed in Ansys. In both simulations,

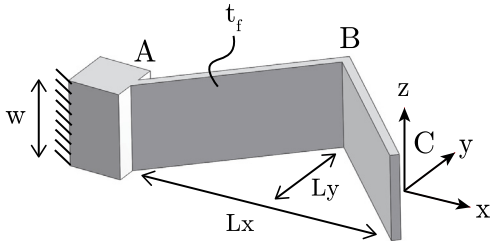

Fig. 9. A folded leaf spring (FLS) with a fixed base.

Table 2
Check of the peak stresses with the Ansys model.

	Rotation angle [deg]	Peak stress Matlab [MPa]	Peak stress Ansys [MPa]	Error [%]
Traditional CFP	+45	209.742	209.517	0.107
	−45	209.742	209.517	0.107
Redesigned CFP	+45	161.295	161.123	0.107
	−45	161.296	161.308	0.007

100 beam elements per flexure were used. Such a large number is not necessary for accuracy but allows to discretize the curved fabrication geometry of the redesigned CFP. The results are shown in Table 2. The maximum error is 0.107%, which can be considered small compared to the stress reduction. Programming scripts containing the two full simulations can be found online using https://doi.org/10.1016/j.precisioneng.2024.05.021. The scripts can be run directly by copy-pasting them in Ansys, providing an easy check of the stress reduction in the CFP.

As a second test, we simulated in Ansys how well the redesigned CFP attains the functional geometry after assembly. In this phase, the flexures should be straight, because the functional geometry has straight flexures. The maximum error in x and y directions of all nodal coordinates (101 per flexure) is 7.577e−4 mm, which can be considered significantly small as compared to the size of the total mechanism.

4. Application example: folded leaf spring with reduced peak stress

In this section we demonstrate the application of the STAGE method for reducing peak stresses in a folded leaf spring (FLS), by using a parameter sweep instead of the graphical approach in step 2 in order to find the optimal force and moment in the release point. This alternative approach can be useful if a desired stress field cannot be determined, or if the mechanism is too complex to use the graphical approach. The outcomes are then verified by two experimental tests and by Ansys simulations.

4.1. The folded leaf spring

Fig. 9 shows the folded leaf spring (FLS) [24–26]. The FLS can be used to replace a wire flexure [24] and five or six FLS-elements can form a linear guide [24,25]. In such a linear guide, a single FLS performs the up and down motions shown in Fig. 10. The FEM simulations, based on the properties shown in Table 3, show significant peak stresses in the flexure. The highest peak stress in the motion range of ±30 mm of the traditional FLS is 482.6 MPa.

4.2. Redesign with the STAGE method and a parameter sweep

The goal here is to reduce peak stresses in the FLS while keeping its functional geometry unchanged. Therefore, we define the FLS design in Fig. 9 as the functional geometry in step 1 of the STAGE method. Step 2 is the design of a stress field and modeling of this field by a

Table 3
Properties of the folded leaf spring in Fig. 9, used for analysis.

Lx	100 mm
Ly	50 mm
w	20 mm
t_f	0.5 mm
Young's modulus	114 GPa
Poisson's ratio	0.33

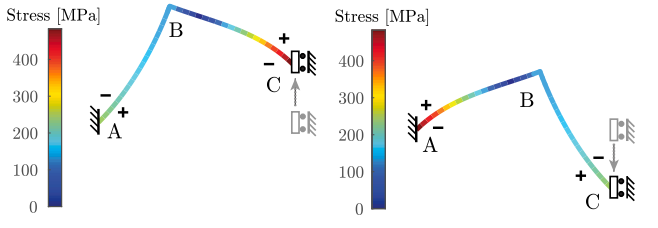

(a) After +30 mm displacement. (b) After -30 mm displacement.

Fig. 10. FEM simulations showing high peak stresses (482.6 MPa) in the traditional FLS at large displacements.

force and moment in a release point. We choose point C in Fig. 10 as a release point. We could have chosen any point in the flexure, but point C is a practical choice for assembling the produced geometry. We will use a parameter sweep to find the optimal force and moment in the release point. The parameter sweep is carried out as follows. Different variable sets are defined, each containing different choices for the modeled force, its angle and the modeled moment. For each set, steps 2 to 4 of the STAGE method are carried out, and the peak stresses of the assembled mechanism are analyzed by moving it up and down ±30 mm, as shown in Fig. 10. The variable set resulting in the lowest peak stress is selected as a final result. Note that each set results in a different stress field, but in the same functional geometry.

4.3. Optimal redesigned FLS

Fig. 11 shows the optimal FLS design resulting from the parameter sweep with a peak stress of 347.1 MPa during motion, which is a reduction of 28% as compared to the traditional FLS in Fig. 10. Fig. 11(a) shows its stress-free fabrication geometry and Fig. 11(b) shows the FLS after assembly. The peak stress of 347.1 MPa is reached in the extreme positions of ±30 mm shown in Figs. 11(c) and 11(d). The modeled force, force angle and moment in the release point corresponding to this design are respectively 6.76 N, 90.5° (approximately horizontal as shown in Fig. 11(a)), and 97.72 N mm.

It is noted that a similar stress reduction cannot be achieved by simply shifting the motion range of the traditional FLS. The traditional FLS experiences the same peak stress in both the up and down positions due to its symmetry along the vertical axis. Shifting the motion range will result in a lower peak stress in one direction, but in a higher peak stress in the other direction.

4.4. Experimental validation of the peak stress reduction

The peak stress reduction in the FLS was validated by measuring the reaction forces and reaction moment in the attachment point A in Fig. 12 during motion, and comparing these to the FEM simulation data. This indirect approach is possible since the stresses throughout the entire FLS are determined by the reaction forces and reaction moment because the FLS is a statically determinate structure, as was explained in Section 2.2.

Both the traditional and redesigned FLS were fabricated from Titanium grade 5 using Wire Electrical Discharge Machining (WEDM). The properties of the traditional FLS are shown in Table 3. The redesigned

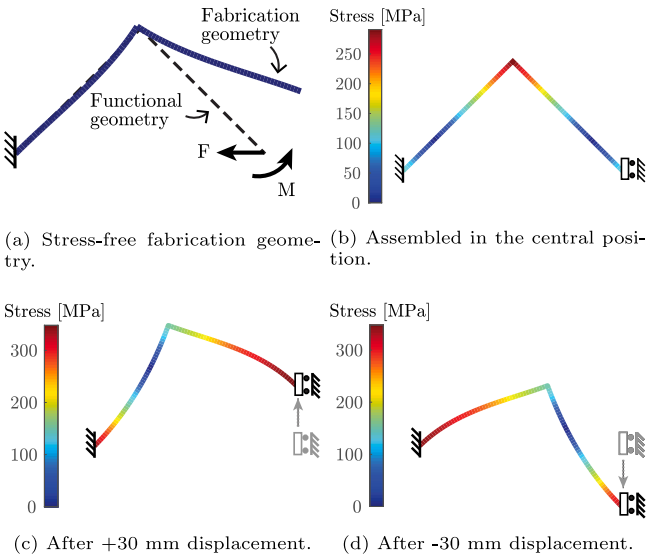

(a) Stress-free fabrication geometry. (b) Assembled in the central position. (c) After +30 mm displacement. (d) After -30 mm displacement.

Fig. 11. The redesigned folded leaf spring, showing a reduced peak stress of 28% as compared to the traditional FLS. This peak stress reduction cannot be achieved by shifting the motion range.

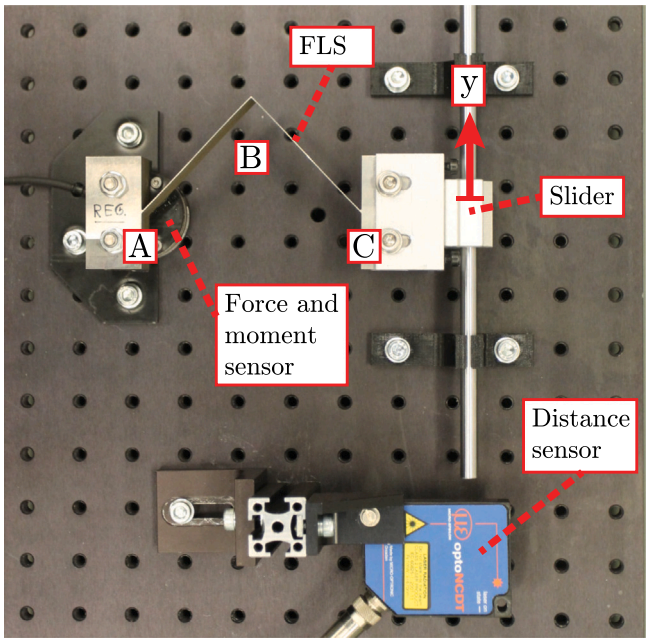

Fig. 12. Experimental setup used to validate the stress reduction by measuring the reaction forces and the reaction moment of the traditional and the redesigned FLS.

FLS has the same width w and thickness t_f, but has a curved fabrication geometry shown in Fig. 11(a), of which the data of the detailed shape is made available online. Fig. 12 shows the setup used to measure the reaction forces and reaction moments of the FLS during motion. Point A of the FLS is attached to the base via a six degrees-of-freedom force and moment sensor (ATI MINI40-SI-40-2). Point B of the FLS is attached to a slider. The slider allows a rotation along its motion axis, which is needed to avoid forces due to misalignments. The displacement of the slider in the y-direction is measured by an optical triangulation sensor (optoNCDT 1420). Both sensors are connected to a data acquisition unit (NI USB-6008) and a laptop for recording. In the experiments the slider was moved up and down four times slowly, to eliminate the influence of dynamic effects.

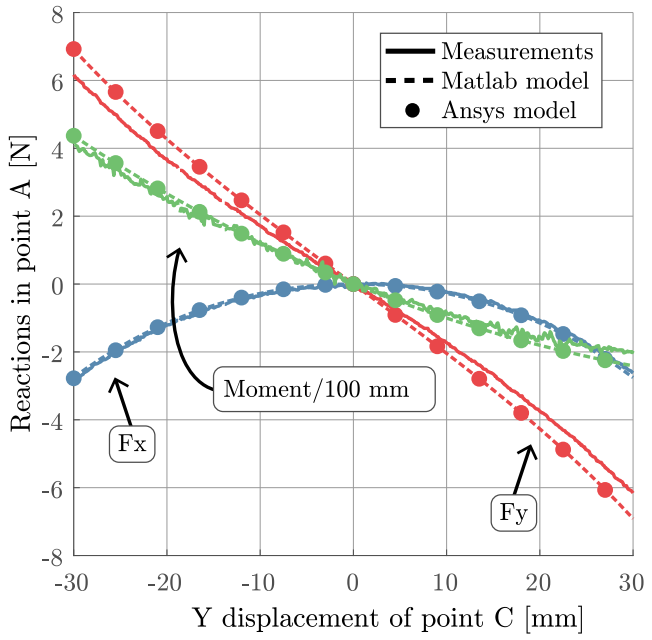

Fig. 13. Experimental results of the traditional FLS compared to the two FEM models, showing a maximum NMAE of 6.0%.

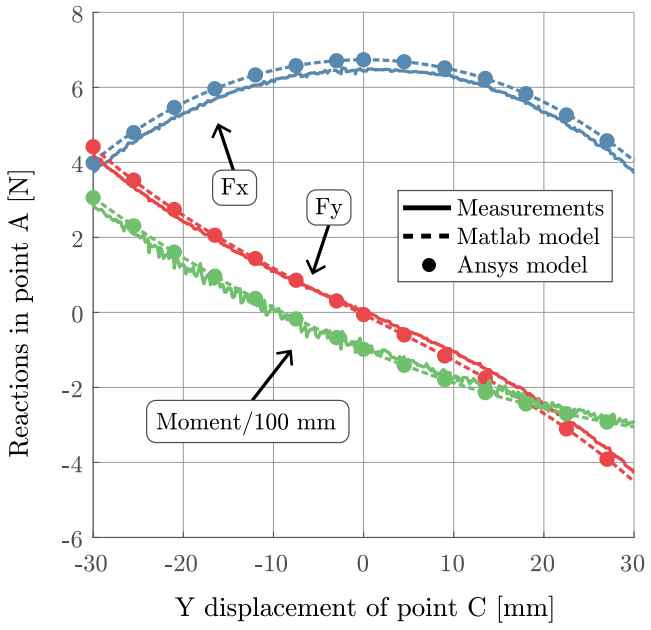

Fig. 14. Experimental results of the redesigned FLS, compared to the two FEM models, showing a maximum NMAE of 5.5%.

The mean of the measured reactions is taken as outcome. A Normalized Mean Absolute Error (NMAE) between model and experiment was computed, which is a regular MAE normalized by the maximum force:

$$\text{NMAE} = \frac{\frac{1}{N}\sum_{n=1}^{N}\left|\hat{\zeta}_n - \zeta_n\right|}{\max|\zeta|}, \tag{10}$$

in which N is the number of measured data points (at least 1500 in all measurements), $\hat{\zeta}$ the measured force and moment values and ζ the values predicted by the FEM model written in Matlab. Fig. 13 shows the experimental results of the traditional FLS design. The moment is divided by a characteristic length of 100 mm (the dimension of the FLS in x-direction) to make it compatible with the reaction forces. The NMAE between the FEM model in Matlab and the measurements of F_x, F_y, and $M/100$ mm are 4.4%, 6.0% and 4.4%, respectively. Fig. 14 shows the results of the redesigned FLS, together with the FEM data. Here, the NMAE between the FEM model in Matlab and the measurements of F_x, F_y and $M/100$ mm are 4.0%, 3.7% and 5.5%, respectively. The deviations between the experiments and the FEM models could be due to fabrication errors: a thickness variation in the flexures of 16 μm on the nominal thickness of 0.5 mm results in an error in the reaction force or reaction moment of 10%, due to the cubic relation between bending stiffness and flexure thickness. The stresses in the FLS scale proportionally to the reaction forces and reaction moments because bending stresses dominate and these scale proportional to force and moment. We conclude that the experiments validate the FEM models and thereby validate the peak stress reduction.

The errors between the Ansys model and the Matlab model are in the same order of magnitude of the round-off error (1e−3 mm), which occurs when exporting the data.

4.5. Experimental validation of the functional geometry

The goal of the second experiment is to measure how well the redesigned FLS obtains its functional geometry after assembly. Fig. 15(a) shows the fabricated geometry of the redesigned FLS, while Fig. 15(b) shows the geometry after assembly, where it has obtained its functional geometry. In this evaluation, we will measure the straightness of the flexures from the images for both the redesigned and the traditional FLS as a reference case. The images are processed as follows: first, two straight, connected line segments are drawn through the points A, B and C in Fig. 15(b). The line segments are fitted such that a maximum straightness results. Then, the deviations of the flexure edges with respect to these lines are plotted. The high-resolution pictures will be published online. Fig. 16 shows the results for both the traditional and the redesigned FLS. Both plots show that the straightness deviation is smaller than half the thickness of the flexure. This can be considered significantly small as compared to the deflections of the flexures during motion.

Additionally, the functional geometry is checked using Ansys. The fabrication geometry of the redesigned FLS is imported and virtually assembled. Using “Beam 188” elements and the nonlinear analysis option enabled, the resulting maximum geometric error is 1e−3 mm, which is of the same order of magnitude as the round-off error due to exporting the data.

5. Discussion

The main idea behind the STAGE method is to consider the functional geometry and the fabrication geometry of a flexure mechanism as separate things. In current literature, the “design of a flexure mechanism” refers to the functional geometry and also serves directly as the drawing for fabrication. This leads to the implicit assumption that the flexure mechanism on the drawing board is always stress-free, which is unnecessary and limits the solution space, as shown in this article by the redesigns of the CFP and the FLS.

Current CFP and FLS elements in machines could be directly replaced by the redesigned versions in this article because their attachment points remain unchanged. In fact, the replacement will not be visible to the naked eye because the only difference is that stresses are introduced. The WEDM fabrication technique used in this paper is commonly used for the production of flexure mechanisms in industry. This means that the curved geometries can also be produced using current production techniques.

This article showed the application of the STAGE method for peak stress reduction, but it could be used for other purposes. For example, actuation forces or eigenfrequencies could be reduced by designing

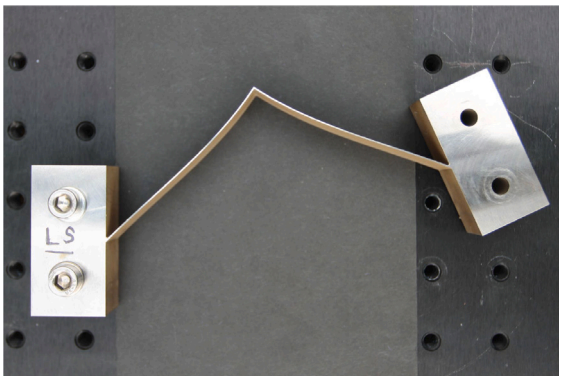

(a)

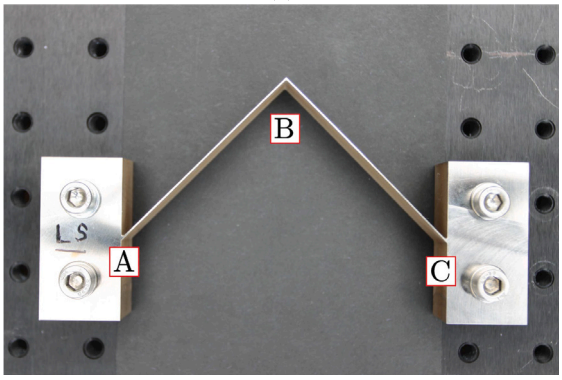

(b)

Fig. 15. The redesigned FLS in stress-free (as-fabricated) state (a) and after assembly in its central position (b).

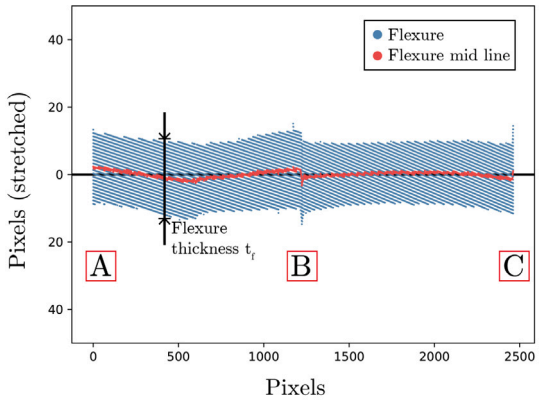

(a) Traditional FLS

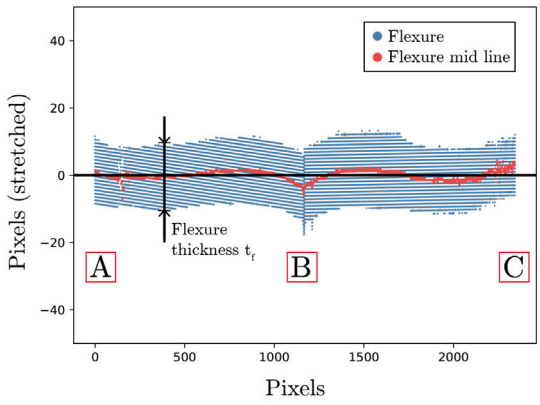

(b) Redesigned FLS after assembly

Fig. 16. Straightness of the traditional (a) and redesigned (b) FLS after assembly, showing that the redesigned FLS attains the functional geometry well after assembly, with a straightness error smaller than half the thickness of the flexures. The mid line shows the straightness, compared to the indicated flexure thickness.

the optimal stress fields, or deformations due to gravity could be mitigated. Furthermore, the functional geometry of the flexure does not necessarily have to be designed in its central position. For example, the functional geometry of the CFP could be designed at a 45° rotation. If the flexures are designed as straight members in this configuration, the flexure will have a high support stiffness at this 45° rotation. The STAGE method can be used to design the geometry of a flexure mechanism anywhere in its motion range.

The designed stresses can only be controlled exactly for a single pose of the mechanism using the STAGE method. In Section 3 we show that despite this, we can decrease the stresses in the full range of motion. The STAGE method does not formally guarantee that this works in all cases.

The STAGE method does not guarantee that each functional geometry with designed internal stresses has a valid corresponding stress-free fabrication geometry. This is because segments of this geometry could intersect, or bifurcations in the displacement path could occur.

The amount of the peak stress reduction which can be achieved using the STAGE method is generally larger when the displacements of the flexures are large. For small displacements, the stress in each point is approximately equal in magnitude in both motion directions, meaning that the STAGE method will be less effective.

The flexures redesigned using the STAGE method are permanently stressed. Therefore a suitable material has to be selected for the mechanism to limit stress relaxation, similar to the design of springs used for permanent pre-stress.

6. Conclusions

In this work we proposed the Stress And Geometry (STAGE) method, to design the geometry and stress of flexure mechanisms simultaneously.

We have demonstrated the method by redesigning the stresses in the well-known crossed-flexure pivot, without changing its functional geometry, which resulted in a peak stress reduction of 23% for ±45° rotation.

Additionally, we showed how peak stresses in a folded leaf spring (FLS) can be reduced by 28%, using a parameter sweep to find the most optimal stress field. This alternative approach can be applied when it is not clear which stress field is most optimal, or if the mechanism is too complex.

The peak stress reduction in the FLS was validated by measuring its reaction forces during motion, showing a maximum normalized mean absolute error between model and experiment of 5.5%.

A second experiment showed that the functional geometry of the FLS is well attained after assembly, with a maximum straightness error of half the flexure thickness.

CRediT authorship contribution statement

Jelle Rommers: Conceptualization, Data curation, Formal analysis, Investigation, Methodology, Validation, Visualization, Writing – original draft, Writing – review & editing. **Volkert van der Wijk:** Conceptualization, Methodology, Supervision, Writing – review & editing, Writing – original draft. **Alejandro M. Aragón:** Formal analysis, Writing – review & editing. **Just L. Herder:** Conceptualization, Funding acquisition, Project administration, Resources, Supervision, Writing – original draft, Writing – review & editing.

Declaration of competing interest

The authors declare that they have no known competing financial interests or personal relationships that could have appeared to influence the work reported in this paper.

Acknowledgment

This work is part of the research program “Möbius” with project number 14665, which is (partly) financed by the Netherlands Organization for Scientific Research (NWO).

Appendix A. Concrete example of the inverse FEM solution method

In this appendix, we provide a concrete example to help to understand the solution method used in the inverse FEM in an intuitive way. First, the example problem is solved analytically. We then use Newton–Raphson to find a solution, similar to the way in which nonlinear FEM problems are often solved. We start with the conventional (forward) case and then show the difference with the inverse case.

Fig. A.17 shows a spring-slider mechanism. The spring with stiffness k is drawn in its stress-free (dashed) and stressed states. We assume that the height h is fixed and the stress-free and stressed geometries of the spring are fully described by x_o and x_s, respectively. We choose $h = 50$ mm, $k = 2$ N/mm, $F_{ext} = 15$ N and $x_o = 25$ mm. The internal force F_{int} is the horizontal component of the spring force, which is equal to F_{ext} at static equilibrium. We write this equilibrium by equating the residual R (the force imbalance) to zero:

$$R(x_o, x_s) = F_{int}(x_o, x_s) - F_{ext} = 0. \tag{A.1}$$

For this example, the following equation can be derived:

$$R(x_o, x_s) = kx_s\left[1 - \sqrt{\frac{h^2 + x_o^2}{h^2 + x_s^2}}\right] - F_{ext} = 0. \tag{A.2}$$

Note that $x_s = x_o + u$, where u is the displacement from the stress-free configuration. Eq. (A.2) is written in terms of x_o and x_s, while conventionally x_o and u would be used. This choice will show to be more convenient for inverse FEM. Eqs. (A.1) and (A.2) already give some insight into the difference between the forward and inverse problem. In the forward case, x_o is known and x_s has to be found, whereas in the inverse case, x_s is known and x_o has to be found.

We now proceed to solve the example problem using the Newton–Raphson solution method, starting with the conventional forward case. We assume that similar to a FEM problem, the analytical equation (A.2) cannot be solved explicitly but its residual can be evaluated sequentially for a certain input x_s. The nonlinear problem can be solved using an iterative gradient-based approach, such as Newton–Raphson. The gradient of the residual equation is computed as:

$$K_{fwd} = \frac{\partial R(x_o, x_s)}{\partial x_s} = k\left[1 - \frac{h^2\sqrt{h^2 + x_o}}{(h^2 + x_s^2)^{3/2}}\right], \tag{A.3}$$

where K_{fwd} is the stiffness of the system. Fig. A.18 shows how this gradient can be used to iteratively find the solution. We start with the (arbitrary) initial guess of $x_s = 30$ mm. The residual is calculated and using K_{fwd} a new guess for x_s is computed. At the intersection of the dashed line with the horizontal axis, this updated value for x_s is obtained and the residual is re-evaluated. This process is repeated until the residual is sufficiently small to consider the problem to be solved. This results in a x_s of around 44.8 mm as the solution to the problem. If we substitute $x_o = 25$ and $x_s = 44.8$ in Eq. (A.2), this indeed results in a residual close to zero.

In the inverse problem, the stressed geometry x_s is known and the stress-free geometry x_o has to be found. We choose $x_s = 44.8$ mm. Using Newton–Raphson, x_o should be found to be close to 25 mm, in order to satisfy the residual equation (A.2). The residual equation is the same as in the forward case. However, the gradient used to solve the problem is different because the residual equation is now a function of x_o:

$$K_{inv} = \frac{\partial R(x_o, x_s)}{\partial x_o} = \frac{-kx_s x_o}{\sqrt{h^2 + x_s^2}\sqrt{h^2 + x_o}}. \tag{A.4}$$

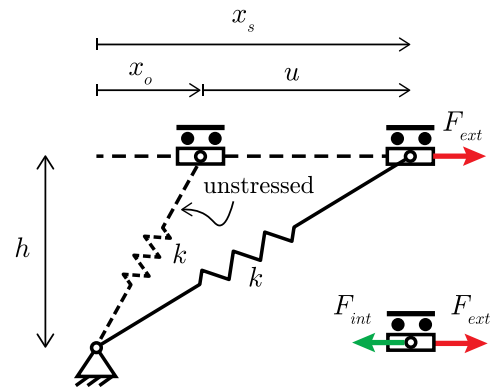

Fig. A.17. Example used to explain the inverse FEM solution method.

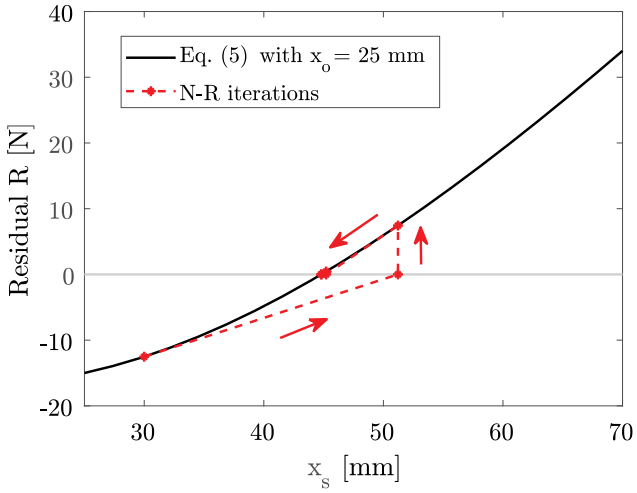

Fig. A.18. Newton–Raphson iterations of the conventional (forward) analysis, in which x_o is known and x_s is to be found. Note that in this case, Eq. (A.2) is a function of x_s.

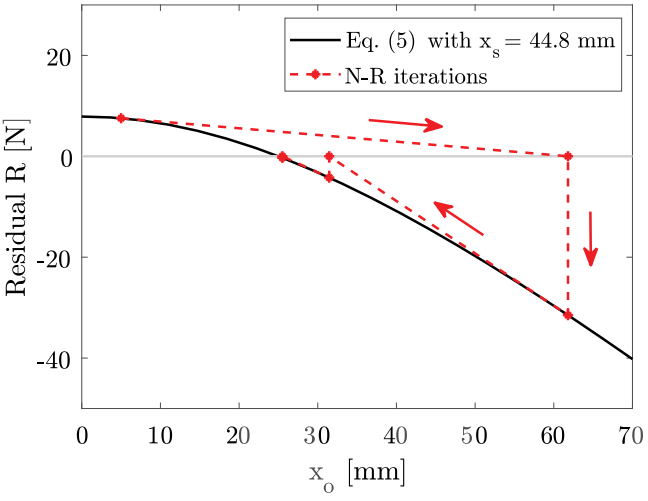

Fig. A.19. Newton–Raphson iterations of the inverse analysis, in which x_s is known and x_o is to be found. Note that in this case, Eq. (A.2) is a function of x_o.

Fig. A.19 shows how this gradient can be used to iteratively arrive at the correct solution of x_o around 25 mm, starting from an arbitrary initial guess of $x_o = 5$ mm.

Crucially, we can now also start at 44.8 mm, change F_{ext} as desired, and find the new unstressed geometry x_o. This is analog to the STAGE method in the article: we change the unstressed geometry by modeling an external force and/or moment on the stressed geometry.

Appendix B. Supplementary data

Supplementary material related to this article can be found online at https://doi.org/10.1016/j.precisioneng.2024.05.021.

References

[1] Hopkins JB, Culpepper ML. Synthesis of multi-degree of freedom, parallel flexure system concepts via freedom and constraint topology (fact)–part I: Principles. Precis Eng 2010;34(2):259–70.

[2] Hopkins JB, Culpepper ML. Synthesis of multi-degree of freedom, parallel flexure system concepts via freedom and constraint topology (fact). part II: Practice. Precis Eng 2010;34(2):271–8.

[3] Hale LC. Principles and techniques for designing precision machines. Tech. rep., Livermore, CA (United States): Lawrence Livermore National Lab.(LLNL); 1999.

[4] Howell LL. Compliant mechanisms. In: 21st century kinematics. Springer; 2013, p. 189–216.

[5] Kim CJ, Kota S, Moon Y-M. An instant center approach toward the conceptual design of compliant mechanisms. 2006.

[6] Kim CJ, Moon Y-M, Kota S. A building block approach to the conceptual synthesis of compliant mechanisms utilizing compliance and stiffness ellipsoids. J Mech Des 2008;130(2).

[7] Radaelli G, Gallego JA, Herder JL. An energy approach to static balancing of systems with torsion stiffness. J Mech Des 2011;133(9).

[8] Gallego JA, Herder J. Synthesis methods in compliant mechanisms: An overview. In: ASME 2009 international design engineering technical conferences and computers and information in engineering conference. American Society of Mechanical Engineers Digital Collection; 2009, p. 193–214.

[9] Burgoyne C, Dilmaghanian R. Bicycle wheel as prestressed structure. J Eng Mech 1993;119(3):439–55.

[10] Awtar S, Quint JM. In-plane flexure-based clamp. Precis Eng 2012;36(4):658–67.

[11] Jensen BD, Howell LL. Bistable configurations of compliant mechanisms modeled using four links and translational joints. J Mech Des 2004;126(4):657–66.

[12] Stacey JP, O'Donnell MP, Schenk M. Thermal prestress in composite compliant shell mechanisms. J Mech Robot 2019;11(2).

[13] van Eijk J, Dijksman JF. Plate spring mechanism with constant negative stiffness. Mech Mach Theory 1979;14(1):1–9.

[14] Hoetmer K, Woo G, Kim C, Herder J. Negative stiffness building blocks for statically balanced compliant mechanisms: design and testing. J Mech Robot 2010;2(4).

[15] Gomez JF, Booker JD, Mellor PH. 2D shape optimization of leaf-type crossed flexure pivot springs for minimum stress. Precis Eng 2015;42:6–21.

[16] Krishnan G, Kim C, Kota S. A metric to evaluate and synthesize distributed compliant mechanisms. J Mech Des 2013;135(1).

[17] Trease BP, Moon Y-M, Kota S. Design of large-displacement compliant joints. 2005.

[18] Wittrick W. The theory of symmetrical crossed flexure pivots. Aust J Chem 1948;1(2):121–34.

[19] Haringx J. The cross-spring pivot as a constructional element. Flow Turbul Combust 1949;1(1):313.

[20] Seelig F. Flexural pivots for space applications. 1968.

[21] Hibbeler RC, Fan S. Statics and mechanics of materials. Vol. 2, Prentice Hall Upper Saddle River; 2004.

[22] Govindjee S, Mihalic PA. Computational methods for inverse finite elastostatics. Comput Methods Appl Mech Engrg 1996;136(1–2):47–57.

[23] Albanesi AE, Pucheta MA, Fachinotti VD. A new method to design compliant mechanisms based on the inverse beam finite element model. Mech Mach Theory 2013;65:14–28. http://dx.doi.org/10.1016/j.mechmachtheory.2013.02.009.

[24] Soemers H. Design principles for precision mechanisms. T-Pointprint; 2011.

[25] Bos A. Position actuator for the elt primary mirror (Ph.D. thesis), The Netherlands: Eindhoven University of Technology; 2017.

[26] Cacace L. An optical distance sensor: tilt robust [.]. (Ph.D. thesis), The Netherlands: Eindhoven University of Technology; 2009.